UNCLASSIFIED

DTIC FILE COPY

AD-A199 695

CUMENTATION PAGE

Form Approved
OMB No. 0704-0188

1b. RESTRICTIVE MARKINGS

2a. SECURITY CLASSIFICATION AUTHORITY

3. DISTRIBUTION/AVAILABILITY OF REPORT
Approved for Public Release; distribution is unlimited.

2b. DECLASSIFICATION/DOWNGRADING SCHEDULE

4. PERFORMING ORGANIZATION REPORT NUMBER(S)

5. MONITORING ORGANIZATION REPORT NUMBER(S)
AFATL-TR-88-123

DTIC ELECTE SEP 28 1988 S D E

6a. NAME OF PERFORMING ORGANIZATION	6b. OFFICE SYMBOL (If applicable)	7a. NAME OF MONITORING ORGANIZATION
Aerodynamics Branch Aeromechanics Division		

6c. ADDRESS (City, State, and ZIP Code)	7b. ADDRESS (City, State, and ZIP Code)
Air Force Armament Laboratory Eglin Air Force Base, FL 32542-5434	

8a. NAME OF FUNDING/SPONSORING ORGANIZATION	8b. OFFICE SYMBOL (If applicable)	9. PROCUREMENT INSTRUMENT IDENTIFICATION NUMBER
Aeromechanics Division	AFATL/FXA	

8c. ADDRESS (City, State, and ZIP Code)	10. SOURCE OF FUNDING NUMBERS			
	PROGRAM ELEMENT NO.	PROJECT NO.	TASK NO.	WORK UNIT ACCESSION NO.
Air Force Armament Laboratory Eglin Air Force Base, FL 32542-5434	61101F	ILIR	86	06

11. TITLE (Include Security Classification)
An Investigation of Controlled Vortex Drag Using Stepped Afterbodies From M = 0.5 to 3.0

12. PERSONAL AUTHOR(S)
Dennis Wikoff, Charles Cottrell, James Packard

13a. TYPE OF REPORT	13b. TIME COVERED	14. DATE OF REPORT (Year, Month, Day)	15. PAGE COUNT
Final	FROM Feb 86 TO Sep 88	September 1988	7

16. SUPPLEMENTARY NOTATION

17. COSATI CODES			18. SUBJECT TERMS (Continue on reverse if necessary and identify by block number)
FIELD	GROUP	SUB-GROUP	
01	01		Base Drag; Separated Flow;
19	10		Projectile Afterbody; Ballistic Testing.

19. ABSTRACT (Continue on reverse if necessary and identify by block number)

A comparison of the zero lift drag coefficients of a stepped base projectile to flat base and truncated boattail base projectiles is presented. Three model configurations were investigated during the test program. These included an experimental 20mm round with a 7 1/2 deg., truncated boattail base, a round modified with a flat base, and a round modified with a stepped base. All of the projectiles were tested at sea level conditions in an indoor ballistic free-flight facility. This paper discusses the aerodynamic experiment and the data obtained. Results show that the zero lift drag coefficient of the stepped base projectile was less than that of the flat base round for the subsonic Mach number range and approximately the same for the transonic and supersonic ranges. However, the stepped base projectile produced zero lift drag greater than that of the boattail round at each Mach number.

Keywords:

20. DISTRIBUTION/AVAILABILITY OF ABSTRACT
☒ UNCLASSIFIED/UNLIMITED ☐ SAME AS RPT. ☐ DTIC USERS

21. ABSTRACT SECURITY CLASSIFICATION
UNCLASSIFIED

22a. NAME OF RESPONSIBLE INDIVIDUAL	22b. TELEPHONE (Include Area Code)	22c. OFFICE SYMBOL
Capt James A. Kidd	(904) 882-4085	AFATL/FXA

DD Form 1473, JUN 86 Previous editions are obsolete.

SECURITY CLASSIFICATION OF THIS PAGE
UNCLASSIFIED

AN EXAMINATION OF CONTROLLED VORTEX DRAG USING STEPPED AFTERBODIES FROM M = 0.5 TO 3.0

Dennis Wikoff*, Charles J. Cottrell**
and
James D. Packard+
Air Force Armament Laboratory
Eglin Air Force Base FL 32542-5434

Abstract

A comparison of the zero lift drag coefficients of a stepped base projectile to flat base and truncated boattail base projectiles is presented. Three model configurations were investigated during the test program. These included an experimental 20mm round with a 7 1/2 deg., truncated boattail base, a round modified with a flat base, and a round modified with a stepped base. All of the projectiles were tested at sea level conditions in an indoor ballistic free-flight facility. This paper discusses the aerodynamic experiment and the data obtained. Results show that the zero lift drag coefficient of the stepped base projectile was less than that of the flat base round for the subsonic Mach number range and approximately the same for the transonic and supersonic ranges. However, the stepped base projectile produced zero lift drag greater than that of the boattail round at each Mach number.

Nomenclature

A = reference area

a = coefficient in Equation 8

C_{Dt} = total drag coefficient

C_{Do} = zero lift drag coefficient (see Equations 7 and 8)

C_{D2} = second order drag term (see Equation 7 and 8)

C_{D4} = fourth order drag term (see Equation 8)

C_{DV} = drag variation due to velocity change (see Equation 8)

e = exponential

M = Mach number

m = model mass

v = velocity along down range axis

x = down range distance

δ = total angle of attack

ρ = air density

δ^2 = effective angle of attack squared

Introduction

A recently published method, by Kentfield, for controlling separated flows to reduce base drag has been investigated in a wind tunnel test.[1-2] This technique involves the formation of captive vortices which induce the flow field to follow the contours of a blunt afterbody that would normally preclude attached flow. It was reported in Reference 1 that the low speed drag on an axisymmetric body with a flat base can be significantly reduced by arranging the afterbody as a series of descending steps followed by a hollow base (Figure 1a). The presence of the steps induces vortex formation which guides the flow smoothly along the afterbody, thereby reducing drag. These experiments seemed to confirm the concept for an axisymmetric body and for a generic fuselage at low subsonic Mach numbers. Drag reductions as high as 56 percent were reported for an axisymmetric model with a stepped afterbody compared with the drag generated by an identical forebody with a conical afterbody of the same length as the stepped configuration.[2]

The objective of the present effort is to investigate further the use of stepped afterbodies in reducing aerodynamic drag. This objective was accomplished by obtaining experimental free-flight data to compare the zero lift drag for axisymmetric configurations on stepped, flat, and boattailed afterbodies (see Figures 1a, 1b, and 1c) in the high subsonic, transonic, and supersonic Mach regimes. This paper presents the results of that effort.

Facilities, Models, and Test Conditions

Free-Flight Range

The free-flight tests were conducted in the Air Force Armament Laboratory's Aeroballistic Research Facility.[3] This facility is an enclosed, atmospheric, instrumented, concrete structure used to investigate the exterior ballistics of various free-flight configurations. The facility contains a gun room, control room, model measurement room, blast chamber, and the instrumented range.

The 207 meter instrumented length of the range has a 3.66 meter square cross section for the

* 1Lt, USAF, Aeromechanics Division, Member AIAA
** Aerospace Engineer, Aeromechanics Division, Senior Member AIAA
+ Cooperative Engineering Student, Auburn University Aerospace Engineering, Student Member AIAA

first by meters and a two meter square cross section for the remaining length. The range has 131 locations available as instrumentation sites. Each location has a physical separation of 1.52 meters, and presently 50 of the sites are used to house fully instrumented orthogonal shadowgraph stations. The maximum shadowgraph window, an imaginary circle in which a projectile in flight will cast a shadow on both reflective screens, is 2.13 meters in diameter. A laser-lighted photograph station is located in the uprange end of the instrumented section. This photographic station yields four orthogonal photographs, permitting a complete 360 deg. view of the projectile as it passes the station on its downrange trajectory. Also, a direct shadowgraph station, consisting of a spark gap and film holder, is located in the uprange end of the test section. Since the film is illuminated directly by the spark as the model passes the station, high quality flow photographs are obtained. The nominal operating temperature of the range is 22 deg. Celsius.

Models and Test Conditions

To achieve the objective of verifying wind tunnel data indicating a subsonic drag reduction, the stepped configuration was chosen from Reference 2 that wind tunnel testing showed to have produced the least drag. This aft section consisted of two steps and a hollow ring of length 0.17 calibers and outside diameter of 0.42 calibers (Figure 1a). A photograph of this base configuration is also included in Figure 2. There was no attempt in this test or in the previous wind tunnel tests to optimize the step shape or dimensions.

A flat base, (Figure 1b), was tested as a control configuration. Both configurations were heavily tested at the subsonic and low transonic Mach numbers to provide well-defined drag curves in these regions. A 7 1/2 deg. truncated boattail the same length as the stepped configuration minus the hollow ring (Figure 1c) was tested at both a subsonic and supersonic Mach number for drag comparison. The boattail slope of 7 1/2 deg. was chosen because that angle is known to be near optimum for reducing the drag of spinning projectiles.[4]

Of particular interest for this research was the affect of a stepped afterbody on the drag of a typical spinning inventory round. An experimental 20mm round was chosen as the projectile because it is representative of operational ammunition and is well suited for both low and high speed testing. Each of the three base sections were machined from a single piece of aluminum and threaded into the base of the 20mm round. Approximately 70 models were flown in the facility during the test program; 50 flights were completely successful, the measured trajectories analyzed, and drag coefficients extracted. The tests were conducted at atmospheric pressure over a Mach number range of 0.52 to 3.14. All testing was conducted using a standard 20mm Mann barrel.

The use of a spinning model required consideration of issues of compatibility between the free-flight and wind tunnel data sets. Namely, these differences necessitated by free-flight tests were: the spin rate of the projectile, higher Reynolds numbers, higher subsonic Mach numbers, and a rotating band near the rear of the round that can act as a trip ring. After careful examination of the wind tunnel test conditions and boattail data, it was believed that the effect of the different testing environments would not obviate the affect of the flow over the base. Also, although the percent of the drag reductions may not be identical, the basic trends should be the same.

Free-Flight Data Reduction

The direct measurements obtained in free-flight testing are the distance traveled as a function of time and the instantaneous angle-of-attack. The relationship between total drag coefficient (C_{Dt}), distance traveled, and the time of flight is then defined by the linear momentum equation,

$$\dot{v} = \ddot{x} = -\frac{\rho A}{2m}\dot{x}^2 \; C_{Dt} \tag{1}$$

where the angle between the velocity vector and the x axis is assumed small. At this point, two methods were employed to determine the zero angle-of-attack drag coefficient (C_{Do}). The first is the classical linear theory techniques.[5,6]

This technique assumes that the basic time and distance measurements can be related by the polynomial function,

$$t = a_o + a_1 x + a_2 x^2 + a_3 x^3 \tag{2}$$

Therefore,

$$\frac{dt}{dx} = a_1 + 2a_2 x + 3a_3 x^2 \tag{3}$$

or

$$\dot{x} = v = \frac{dx}{dt} = \frac{1}{a_1 + 2a_2 x + 3a_3 x^2} \tag{4}$$

then,

$$\ddot{x} = -\frac{2a_2 + 6a_3 x}{(a_1 + 2a_2 x + 3a_3 x^2)^2} \tag{5}$$

By recognizing that $\dot{v} = \frac{dv}{dt} = \frac{dv}{dx}\frac{dx}{dt}$, substituting Equations (4) and (5) into Equation (1), and rearranging, we arrive at

$$C_{Dt} = \frac{2m}{\rho A}\frac{2a_2 + 6a_3 x}{a_1 + 2a_2 x + 3a_3 x^2} \tag{6}$$

Therefore, using Equation (2), the a_1 coefficients are determined by fitting the measured time and distance values. Then, using the determined a_1 coefficients, C_{Dt} can be evaluated at the mid-range distance (x_{mr}) by using Equation (6). The zero lift drag coefficient (C_{Do}) is then obtained by assuming that the total drag coefficient is a quadratic function of the effective angle of attack squared, or,

$$C_{Do} = C_{Dt} - C_{D2}\delta^2 \tag{7}$$

where the value used for C_{D2} in this study was 0.0008/deg^2 (slope of C_{Dt} versus δ^2 curve). The C_{Do} values obtained using this technique are shown in Table 1.

Table 1. Experimental drag results

Config.	Mach No.	Re $\ell \cdot 10^{-6}$	C_{Dt}	δ^2	C_{Do}
Stepped	1.265	6.83	0.609	8.34	0.602
	1.308	7.10	0.594	6.44	0.589
	0.730	4.02	0.272	4.41	0.268
	0.775	4.22	0.304	7.27	0.298
	0.860	4.69	0.326	0.42	0.325
	1.405	7.62	0.542	6.09	0.537
	2.075	11.39	0.455	4.90	0.451
	1.895	10.45	0.472	1.05	0.471
	1.902	10.47	0.467	2.80	0.465
	3.071	16.88	0.330	9.14	0.323
	3.057	16.88	0.331	1.92	0.329
	3.040	16.81	0.346	25.01	0.326
	0.849	4.69	0.304	5.73	0.299
	0.804	4.45	0.377	25.49	0.357
	0.604	3.27	0.358	99.89	0.278
	0.658	3.57	0.276	2.81	0.274
	0.633	3.43	0.271	5.36	0.267
	0.613	3.34	0.298	4.63	0.294
	0.607	3.29	0.336	45.29	0.300
	0.955	5.24	0.443	7.61	0.437
	0.946	5.11	0.401	7.79	0.395
	0.992	5.41	0.540	14.47	0.528
	0.915	4.99	0.381	11.67	0.370
Flat	0.870	4.72	0.354	6.17	0.349
	0.456	2.48	0.347	26.62	0.326
	1.066	5.80	0.434	11.37	0.425
	0.744	4.05	0.374	10.67	0.365
	0.928	5.05	0.376	12.96	0.366
	1.268	6.90	0.665	0.79	0.664
	1.265	6.87	0.608	6.93	0.602
	1.261	6.84	0.632	10.01	0.624
	1.901	10.47	0.458	1.77	0.456
	2.048	11.28	0.440	4.43	0.436
	1.928	10.62	0.454	2.02	0.452
	3.133	17.32	0.327	8.36	0.320
	3.141	17.38	0.312	4.09	0.309
	3.144	17.38	0.315	2.11	0.313
	0.867	4.78	0.368	7.84	0.362
	0.766	4.22	0.335	10.81	0.326
	0.655	3.547	0.341	9.13	0.334
	0.660	3.580	0.341	14.81	0.329
	0.583	3.165	0.359	8.26	0.352
	0.723	3.940	0.355	9.70	0.347
	0.776	4.206	0.333	5.82	0.328
	1.054	5.706	0.576	3.42	0.573
	1.132	6.176	0.630	8.51	0.623
Boattail	2.915	15.855	0.337	0.48	0.336
	2.900	15.744	0.324	6.07	0.319
	0.489	2.668	0.271	60.93	0.222
	0.537	2.912	0.295	105.91	0.210
	0.518	2.810	0.278	35.71	0.249
	0.516	2.787	0.217	3.63	0.214

The second method used for this study involved numerically integrating Equation (1) and expanding C_{Dt} into the continuous function,

$$C_{Dt} = C_{Do}\, e^{\delta a} + C_{D2}\, \delta^2 + C_{D4}\, \delta^4 + C_{DV}\, (\dot{x}\text{-}Vref) \quad (8)$$

The a, C_{D2} and C_{D4} coefficients account for drag due to angle of attack, and the C_{DV} term accounts for variations in drag coefficients with Mach number and Reynolds number.[7] The Mach number-Reynolds number effects cannot be easily separated because they both depend linearly on velocity.

The unknown coefficients in the C_{Dt} expansion are determined by fitting the measured time and distance data with the numerical solution of Equation (1). The fitting process is a least squares technique with the angle-of-attack history provided as input. This method, described by Chapman and Kirk[8], parametrically differentiates the equation of motion, Equation (1), with respect to each of the unknown coefficients shown in Equation (8). Numerical integration of the equation of motion and the parametric equations are then used to match the theoretical equation of motion to the experimental time and distance measurements.

Flights of the same configuration were analyzed using a multiple fit technique over Mach number ranges which corresponded to small changes in the drag curve slope. This provided a common set of aerodynamic coefficients that matched each of the separately measured position-time-altitude profiles. The multiple fit approach increases the probability that the determined drag coefficient best matches that of each flight over the entire range of test conditions assuming that there are no physical differences between models.

Results and Discussion

The zero lift drag coefficients obtained from the experimentally measured data using the classic linear method, Table 1, are plotted as a function of Mach number for all three configurations in Figure 3a-c. The expansion of C_{Dt} (Equation 8) and subsequent multiple fits using the numerical integration techniques of Reference 8 were employed in an attempt to reduce the data scatter for each configuration. However, this method assumes that each projectile of the same configuration has the same C_{Do} for a given Mach number. Since the projectile body consisted of an experimental round and was not precision machined, there were slight variations in the configurations, especially the nose region. In addition, inflight photographs of the projectiles (Figure 5a-c) revealed that the plastic rotating band had 'burred' in places and was protruding into the flow. This was particularly severe for the subsonic Mach numbers where the data scatter is the worst. At higher speeds, the burrs were stripped off early in the flight. These anomalies caused variations in C_{Do} for the same configuration at the same Mach numbers which account for the data scatter in Figure 3, and also caused results for C_{Do} obtained from Equation 8 and the multiple fits to be erroneous. Therefore, although the multiple fit results are not plotted herein they were important in confirming that real physical differences existed from model to model.

The faired curves shown in Figure 3 have been transferred for comparison purposes in Figure 4. This figure shows dramatically that the primary differences in C_{Do} of the three base configurations occur in the subsonic region. In the flat portion of the subsonic drag curve, below M = 0.8, incorporating the aft steps reduces the drag of a flat based projectile by 19 percent. Above M = 0.8 the drag for the stepped base rises sharply. By M = 0.95 the two curves are indistinguishable and there is no apparent difference in the drag of the two projectiles for

the remainder of the Mach number range. The boattail configuration, however, reduces the drag even over the stepped base configuration in both the subsonic and the supersonic region. The addition of the boattail reduces the drag of a flat base configuration by 26 percent in the subsonic region and by 5 percent in the supersonic region.

Figures 5a-c show flow visualization shadowgraphs which present turbulence characteristics of the different bases. Figure 5a shows the boattail round in free flight at M = 0.53. Although no shocks are present, the sudden transition to turbulence is indicative of a flow separation bubble occurring at the round's crimp groove. The turbulent boundary layer appears to follow the curvature of the boattail and evolves into a comparatively narrow wake. Figure 5b shows the flat base configuration at M = 0.60. Here, the evidence of separation at the crimp groove is also apparent and a turbulent wake is clearly shown. The diameter of the flat base round's wake is greater than that of the boattail. This indicates a lower base pressure on the flat base than on the boattail round with a corresponding higher zero lift drag. Figure 5c shows the turbulent wake of the stepped round at M = 0.62. As before, the flow is seen to begin separating at the crimp groove and continues to separate over the steps, contributing to a turbulent wake. However, the wake follows the general contours of the steps, approximating the flow over the boattail and narrowing the wake. As with the boattail, the base pressure is increased and the zero lift drag decreased.

Figure 6a shows both the shock and wake patterns of the flat base configuration at M = 0.94. There is evidence of an expansion wave originating at the shoulder. A strong lambda shock has formed approximately halfway between the shoulder and the base. There appears to be a second lambda shock emerging immediately aft of the first shock. A well-defined wake is also visible. Figure 6b presents the shock structure and the wake region of the stepped round at M = 0.96. This complex flow field includes an expansion at the shoulder, two distinct lambda shocks in the mid-body region, an expansion fan emanating from the steps, and a trailing shock aft of the base. The turbulence that forms the wake seems to originate at the most forward step. However, the wake does not tend to conform to the reduced diameter of each succeeding step as appeared to occur in the M = 0.62 photograph (Figure 5c). Here it seems to maintain a nearly constant diameter indicating similar base pressures.

Finally, it should be noted that the controlled vortex drag reduction phenomena reported by Kentfield[1,2] occurred in incompressible flow where a turbulent wake may not be present. It is believed that the presence of this turbulence diminishes the effectiveness of the stepped afterbody by preventing the captive vortices from developing.

Concluding Remarks

A free-flight comparison of the zero lift drag of stepped base, flat base, and boattail base projectiles has been made. Results indicate that the zero lift drag of the stepped base projectile was 19 percent less than that of the flat base round for the subsonic Mach number range and approximately the same for the transonic and supersonic ranges. The stepped base projectile generated zero lift drag greater than that of the boattail round at each Mach number tested.

References

[1]Kentfield, J.A.C., "Short Multi-Step, Afterbody Fairings," Journal of Aircraft, Vol. 21, No. 5, 1984, pp. 351-352.

[2]Kentfield, J.A.C., "Drag Reduction of Controlled Separated Flows," AIAA Paper 85-1800, August 1985.

[3]Winchenbach, G.L., Galanos, D.G., Kleist, J.S., and Lucas, B.F., "Description and Capabilities of the Aeroballistic Research Facility," AFATL-TR-78-41, April 1978.

[4]Murphy, C. H., Schmidt, "The Effect of Length on the Aerodynamic Characteristics of Bodies of Revolution in Supersonic Flight," Ballistic Research Laboratory, Aberdeen Proving Ground, Rept. 876, August 1953.

[5]Murphy, C.H., "Free-Flight Motion of Symmetric Missiles," Ballistic Research Laboratory, Aberdeen Proving Ground, Rept. 1216, July 1963.

[6]Murphy, C.H., "Data Reduction for Free-Flight Spark Ranges," Ballistic Research Lab, Aberdeen Proving Ground, Rept. 900, February 1954.

[7]Sabot, S.M., Winchenbach, G.L., and Chapman, G.T., "Comparison of Various Drag Coefficient Expansions Using Polynomials and Splines," Journal of Spacecraft and Rockets, Vol. 23, No. 3, 1986, pp. 259-263.

[8]Chapman, G.T., and Kirk, D.B., "A Method for Extracting Aerodynamic Coefficients from Free-Flight Data," AIAA Journal, Vol. 8, April 1970, pp. 753-757.

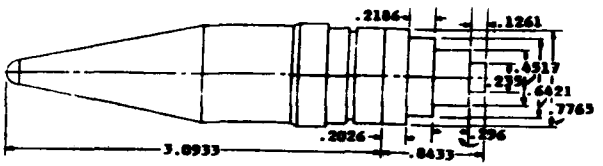

a. Stepped Configuration

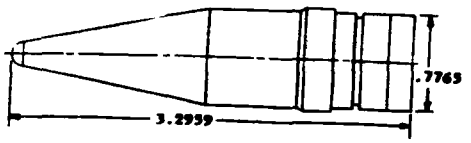

b. Flat Base Configuration

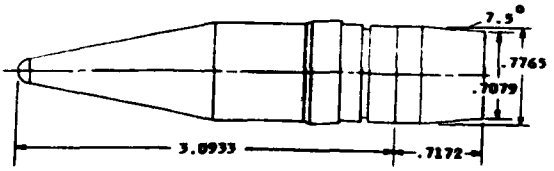

c. Boattail Configuration

Fig. 1 Sketch of model configurations

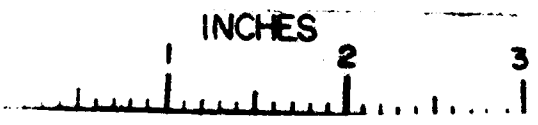

Fig. 2 Photograph of stepped base section

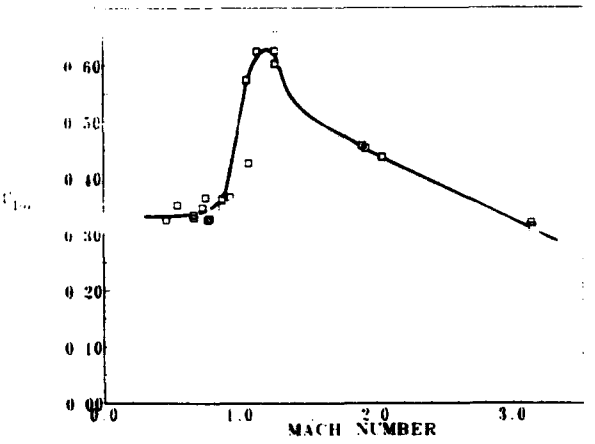

a. Flat base

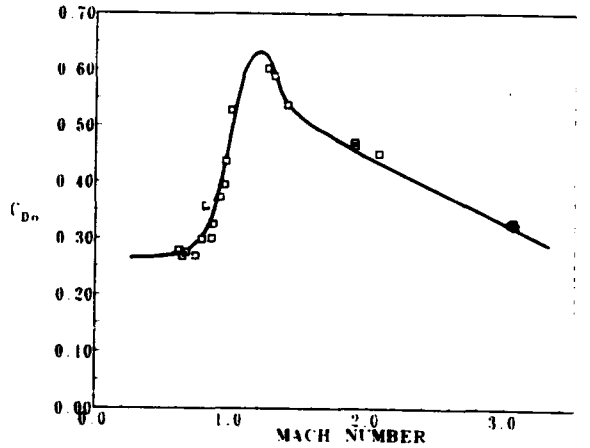

b. Stepped base

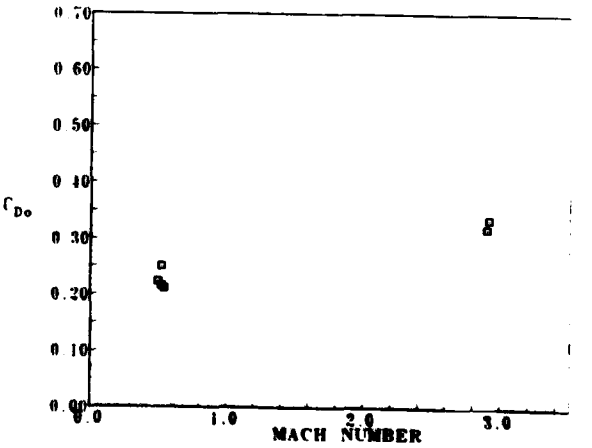

c. Boattail

Fig. 3 Zero lift drag data plots

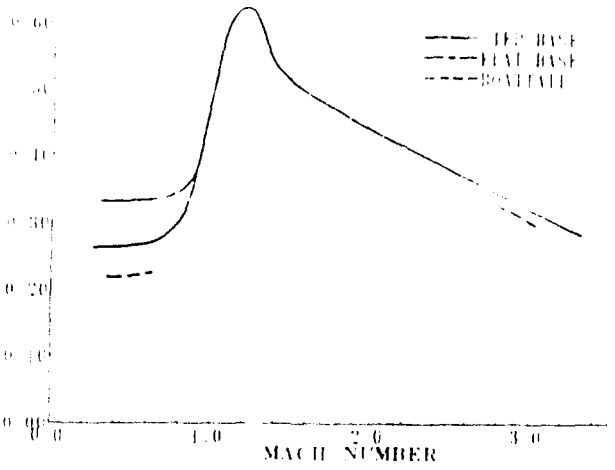

Fig. 4 Zero lift drag comparisons

a. Boattail configuration

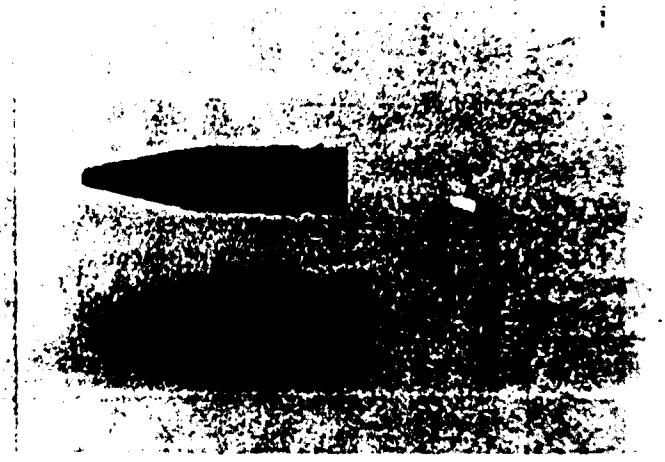

b. Square base configuration

c. Stepped base configuration

Fig. 5 Subsonic flow fields

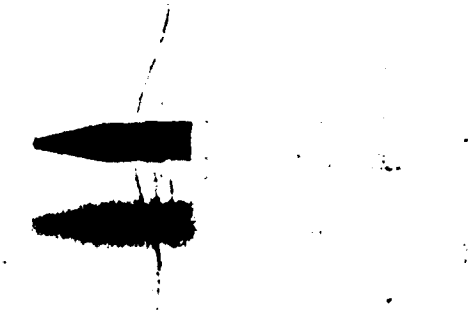

a. Square base

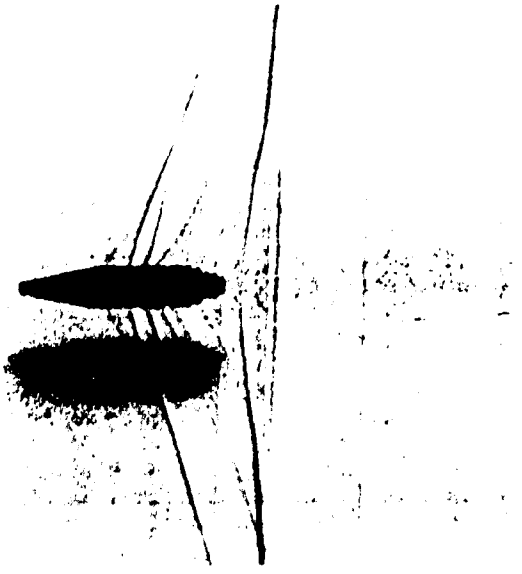

b. Stepped base

Fig. 6 Transonic flow field